Erin Bryce [ORCID] · **Daniela Castro-Camilo · Claire Dashwood · Hakan Tanyas ·
Roxana Ciurean · Alessandro Novellino · Luigi Lombardo**

An updated landslide susceptibility model and a log-Gaussian Cox process extension for Scotland

Abstract At the time of its development, GeoSure was created using expert knowledge based on a thorough understanding of the engineering geology of the rocks and soils of Great Britain. The ability to use a data-driven methodology to develop a national-scale landslide susceptibility was not possible due to the relatively small size of the landslide inventory at the time. In the intervening 20 years, the National Landslide Database has grown from around 6000 points to over 18,000 records today and continues to be added to. With the availability of this additional inventory, new data-driven solutions could be utilised. Here, we tested a Bernoulli likelihood model to estimate the probability of debris flow occurrence and a log-Gaussian Cox process model to estimate the rate of debris flow occurrence per slope unit. Scotland was selected as the test site for a preliminary experiment, which could potentially be extended to the whole British landscape in the future. Inference techniques for both of these models are applied within a Bayesian framework. The Bayesian framework can work with the two models as additive structures, which allows for the incorporation of spatial and covariate information in a flexible way. The framework also provides uncertainty estimates with model outcomes. We also explored consideration on how to communicate uncertainty estimates together with model predictions in a way that would ensure an integrated framework for master planners to use with ease, even if administrators do not have a specific statistical background. Interestingly, the spatial predictive patterns obtained do not stray away from those of the previous GeoSure methodology, but rigorous numerical modelling now offers objectivity and a much richer predictive description.

Keywords Landslide susceptibility · Landslide intensity · Scotland · Log-Gaussian Cox process · Uncertainty estimation

Introduction

Despite being deemed a low-risk country in terms of geological hazards compared to some of its European neighbours (Giles 2020), geohazards in Great Britain (GB) still cause costly delays and disruption to the transport network. For instance, shrink-swell issues alone are estimated to have cost the economy £3 billion over the last decades (British Geological Survey GeoClimate 2022). Landslides, and in particular debris flows (Hungr et al. 2014), also threaten critical infrastructure and human lives, especially in Scotland where slope failures can be large enough to damage local infrastructure, block transport routes, and isolate remote communities (Winter et al. 2010). Numerous disruptive debris flow events have highlighted the continued need to produce usable, applied landslide information, especially in the light of expected climate change impacts. A key information source to reduce the impact of landslides consists of an accurate landslide susceptibility map, which traditionally conveys the spatial probability of a given hazard occurrence conditional on a set of predisposing factors (Van Westen et al. 2008). National-scale landslide susceptibility maps (LSMs) in GB are developed and managed by the British Geological Survey (BGS), as part of the GeoSure digital data product (British Geological Survey GeoSure 2019) which covers 6 main types of potential ground movement which could impact development and existing infrastructure. The LSMs are available for consultation by policy-makers, planners and homebuyers to assess landslide potential and are underpinned by the BGS National Landslide Database (NLD; British Geological Survey NLD 2012), the most extensive source of information on landslides in Great Britain. There are two LSMs, one for debris flows and one for more general landslide processes, both were developed using a heuristic approach where expert knowledge of the terrain provides a user-derived score for specific geological, geomorphological and structural conditions (Ciurean and Lee 2022). Landslide susceptibility mapping has evolved from objective techniques and simple limit equilibrium models to increasingly complex statistical and deep learning approaches; the expansion in the complexity and number of techniques has been matched by an ever-increasing number of publications in the scientific literature (Dong et al. 2023) GeoSure was developed during the 2000's before the National Landslide Database was sufficiently populated to allow for a meaningful quantitative analysis to be undertaken. As with all LSM techniques, there are advantages and disadvantages and without subjective expert judgement, the heuristic GeoSure methodology would not have been able to produce a national-scale LSM at the time. With the NLD now representing a picture of landslide processes across GB, it is possible to explore a quantitative, data-driven approach. The development of data-driven tools has explored several themes with time, through dedicated research on performance-oriented solutions such as machine (Goetz et al. 2015) and deep (Azarafza et al. 2021) learning. Additionally, marked development has made use of dedicated experiments on:

(i) Uncertainty estimation (Tanyas and Lombardo 2020), sampling strategies for (ii) stable (Steger et al. 2016) and (iii) unstable (Chang et al. 2023) slopes, (iv) space–time extensions (Lombardo et al. 2020a, b), as well as (v) bias capture and removal (Steger et al. 2021), and (vi) variable selection (Budimir et al. 2015) among others.

Aside from the themes mentioned above, a very limited literature has been dedicated to adapting the multivariate framework to modelling hazard instead of susceptibility. Specifically, the first

definition of landslide hazard refers to this notion as "the probability of occurrence within a specified period of time and within a given area of a potentially damaging phenomenon", something Guzzetti et al. (1999) later modified to account for the intensity associated to a population of landslides (Crozier 2005). Notably, the intensity of a single landslide, as a measure of its potential threat, can be expressed in terms of its velocity, (Pudasaini and Krautblatter 2022), kinetic energy (Chang et al. 2017) or force (Tang et al. 2014). However, whenever the scale of the study involves large geographic regions, such intensity-related measures are impossible to retrieve due to the costs involved with the geotechnical data acquisition (van den Bout et al. 2021). For this reason, few recent alternatives have been proposed to express landslide intensity over entire landscapes. Specifically, Lari et al. (2014) have proposed an intensity measure for rock falls under the assumption that failure sources are distributed according to a Poisson exponential family. Similarly, Lombardo et al. (2018) proposed a doubly stochastic structure (via a log-Gaussian Cox Process, LGCP) to model the expected number of landslides per mapping unit. Interestingly, from a purely statistical perspective, the product of an LGCP model is denoted as intensity (Illian and Hendrichsen 2010), although this concept is different than landslide intensity which is a function of magnitude and velocity. Furthermore, Taylor et al., (2018) explored the possibility of expressing intensity as a function of landslide length-to-width ratios as a proxy indicator of the runout characteristics. More recently, Lombardo et al. (2021) presented a data-driven solution to the landslide intensity estimation by fitting a log-Gaussian model to global landslide planimetric areal data. The same idea was further polished by Bryce et al. (2022) who proposed a Hurdle model to combine the probability of landslide occurrence with the expected planimetric extent. In this broad context, it becomes evident that no single solution exists to predict landslides and associated characteristics. One of the main determinants of the choice among these solutions has to do with data availability. In fact, most landslide inventories are expressed as point locations, these being diagnostic of where the failure mechanism occurred (Martha et al. 2013). Therefore, the information on the planimetric area is not included as part of the inventory metadata. This is not the case for landslide polygonal inventories (Guzzetti et al. 2012) which are more complex to define. Notably, deep-learning automated solutions have improved the situation in recent years, especially in addressing the need for multi-temporal landslide mapping (Bhuyan et al. 2023). In Great Britain, the BGS has collected both point and polygon data depending on the method of data collection, with polygonal data collected mainly by BGS mapping teams whilst point data is often sourced from social media, news outlets and reports from the public. It was decided to limit the LSM to purely debris flow processes given that they have been the most widely destructive and disrupting landslide process in recent years and create an updated landslide predictive model for Scotland based on an inventory of over 1800 debris flow initiation points. With the available point data, the modelling archetypes available were limited to two options, the first being modelling landslide susceptibility by the given units as per international standard, and the second being the LGCP model by the point pattern of the landslides. The susceptibility framework has the advantage of being widely recognized; in fact, third parties such as insurance companies, councils, and transport (road and railway) agencies can directly use this level of information.

Complimentary, the LGCP model framework provides a point-based solution to predict the rate of landslide occurrences. Here, we implemented both archetypes using the Bayesian paradigm. Specifically, we adopt a latent Gaussian modelling framework using a Bernoulli likelihood for landslide susceptibility and an LGCP for the rate of landslide occurrence. Observations are assumed to be conditionally independent given a latent structure that drives the dependencies and non-stationarities in the data. This latent structure is specified through an additive structure that allows the incorporation of covariate and spatial effects which describe the spatial dependence across observations. This dependence is characterised using the Matérn family of covariance functions, widely used in geostatistics due to its flexible local behaviour and important theoretical properties. Fast and accurate inference for these complex spatial structures is achieved using the stochastic partial differential equation (SPDE; Lindgren et al. 2011) approach. The adapted Bayesian framework is fitted using the integrated nested Laplace approximation (INLA; Rue et al. 2009), which allows us to easily incorporate prior information on the effect of covariates over the responses and provide a thorough description of the quantities of interest and their associated uncertainties. These uncertainties are often underestimated in most geomorphological research, with few notable exceptions (e.g., Korup 2021). This situation is even more prominent at the level of regulators and decision-makers (Hill et al. 2013). For this reason, we also investigate how to combine uncertainty estimates in geostatistical analyses and specifically in their cartographic translation.

The remainder of the manuscript is structured as follows. The "Study area" section describes the study area; the "Data" section details the data used for the analyses later explained in the "Method" section. The "Results" section presents results for each model, and the "Model performance assessment" section presents our model performance assessment. Finally, the "Discussion" and "Conclusions" sections provide discussions and concluding remarks.

Study area

The target of our study is Scotland, a main landmass surrounded by multiple smaller islands covering an area of ~ 80,000 km² (Fig. 1). Most of the British landmass is dominated by a gentle topography with a slope angle of less than 5° characterising 90% of the total territory (Cigna et al. 2014; Novellino et al. 2017). Conversely, the Scottish landscape is characterised by over 50% upland environments formed as a result of an interaction between glacial incisions and post-glacial isostatic uplift (Firth and Stewart 2000). Scotland's diverse bedrock formations are covered by a thin or patchy cover of superficial deposits such as glacial till, hummocky morainic deposits as well as weathered bedrock. Notably, most shallow flow-like landslides take place in such superficial materials. (Palamakumbura et al. 2021). The impact of ice erosion has created several recognizably distinct landscapes across Scotland including the western ice-scoured landscape, weathered bedrock and solifluction deposits in the far east, ice-scoured lowlands and extensively modified valleys, troughs, and mountains (McKirdy and Crofts 1999). Land-use in Scotland is quite homogeneous, with a large percentage of its surface dedicated to agriculture (~ 70%), with woodland corresponding to most of the remaining cover, according to the CORINE Landcover map (CLC; Copernicus 2018). As for
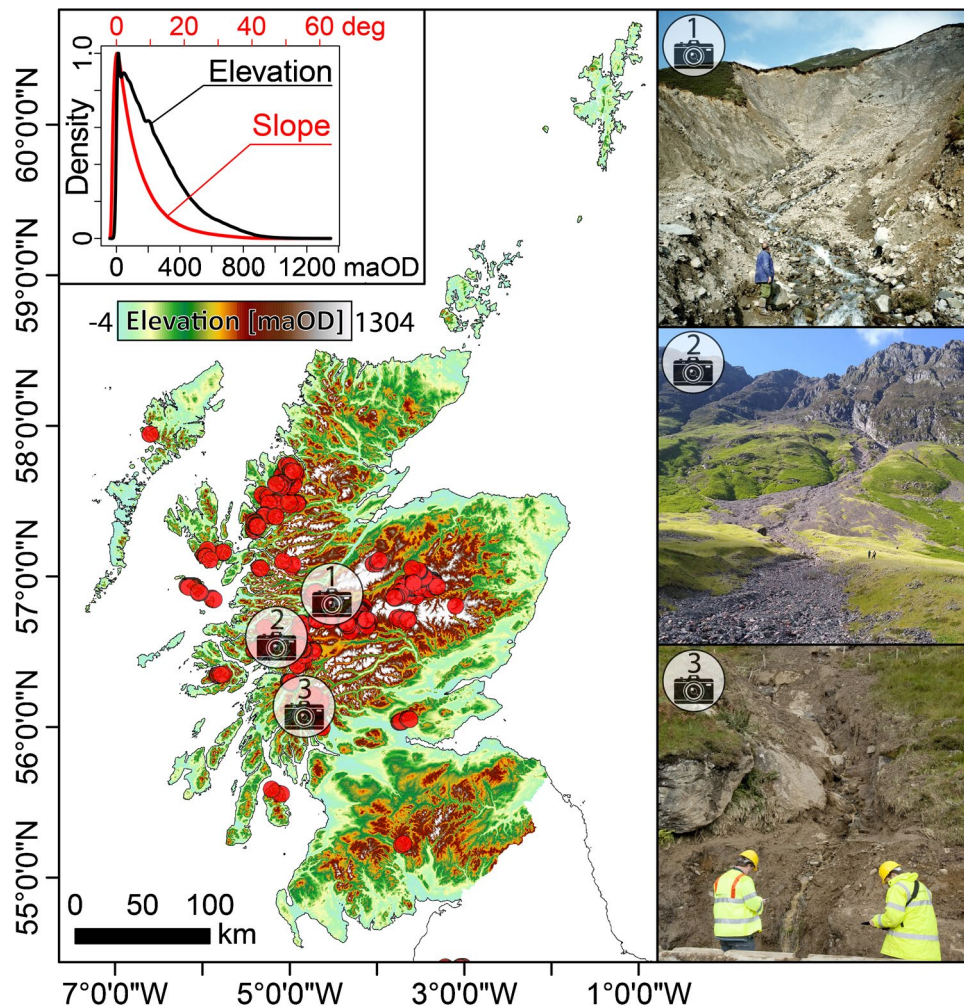
Fig. 1 Terrain overview of Scotland summarised both cartographically and as the two probability density plots for elevation and steepness. The three photos are taken from the BGS field collection of debris flows. The DEM source is NEXTMap Britain elevation data from Intermap Technologies. Photo number #1 is a BGS image P001177© UKRI 1990, photo number #2 is a private photo provided by Katie Whitbread, and photo number #3 is a BGS image P757938© UKRI 2009. Red points indicate the triggering locations of DFs. As for the distributions of elevation and slope, the two densities have been rescaled between 0 and 1

the built-up areas, these occupy a minor extent, with urban classes accounting for less than 3%. The main cities are spread across the central belt and communications among centres are ensured by a road network relying on a few main transport arteries. In places, the lack of diversions away from these key routes makes them sensitive to the occurrence of landslides. The Scottish road and rail networks are regularly affected by debris flows, with the most well-known example of this being the Rest and Be Thankful (RABT). The RABT was closed in October 2023 after being hit by seven landslides in just a few days whilst in the same storm event ten people were air lifted to safety after becoming stuck between landslides on the A83 and A815. Previous heavy rainfall events have led to a debris flow that affected the Fort William to Mallaig train line as well as the A830 highway in 2016 in an area previously considered to be of low debris flow susceptibility (Palamakumbura et al. 2021). Whilst each one of these events was relatively small in scale the impacts on local communities and businesses can be significant, the village of Ardfern for instance remained inaccessible a month after a 6000-tonne landslide blocked the A816 rendering it impassable. The potential for these types of landslides to increase with future climate change highlights the need for modern up-to-date LSMs.

Data

The BGS NLD is a continuously updated source of landslide information (Foster et al. 2012). For this study, we extracted Debris Flow (DF) locations because they are the most common landslide type in Scotland, and they cause the largest impact on infrastructure routes. This is the main reason why in this research, we opted to model precisely this landslide class, as an updated prediction map, which could help address some of the needs to spatially locate DF locations that may affect road and railway infrastructures. Notably, the NLD has changed the way landslides have been collected; initially, BGS would collect information sourced from news reports, and individual and transport institution reports whilst recent developments have seen the use of social media and earth observations from satellite scenes (Pennington et al. 2015). This combined search is meant to ensure

that any potential bias in the spatial distribution of landslides is minimised. Understanding bias is important when dealing with a spatially distributed process such as landslides, the inclusion of earth observations is intended to limit the skew towards transportation routes and urban areas that can be produced by collecting data purely from social media posts and reports from transport infrastructure operators. To further understand the implications of such potentially biased sources, we suggest reading the work of Lima et al. (2021) or Lin et al. (2021). To avoid propagating such biases one could use two potential solutions. The first is in introducing bias-related covariates in the model fitting, which are then zeroed out in the model prediction phase (Lima et al. 2017). The second and alternative solution is to solve the issue at the source by introducing an independent mapping procedure. The strategy of the BGS includes the use of freely available Sentinel-2 satellite images and an approach similar to NASA's Sudden Landslide Identification Product (SLIP) tool (Fayne et al. 2019) to automatically map potential debris flow locations. This combined approach ensures that the NLD reflects the standards of quality (Galli et al. 2008) and completeness (Tanyas and Lombardo 2020) required for a suitable landslide prediction modelling protocol. The resulting inventory features 1,854 DFs across the Scottish mountainous terrain. These DFs have been digitally recorded with a point whose x and y correspond to the highest position visible on the source area.

The reason behind such a choice is to represent the most likely location where the failure was initiated (Scheip and Wegmann 2022). Notably, this may be an approximation because laboratory experiments have proven that DFs may exhibit retrogressive behaviour (Sosio et al. 2007). However, as one faces the limitation of being only able to examine the scarp left by the DF, choosing the highest point along a polygon perimeter is the most reasonable approach (Lombardo et al. 2014). Nevertheless, this level of detail is to be accounted for whenever the mapping unit of interest is expressed at high resolution. At the level of a coarse spatial partition, the assignment of a stable/unstable label would not change (see "Mapping unit choice and dependent and independent variables' assignment" section). In this research, we opted to partition Scotland into Slope Units (SUs) and therefore, no substantial changes are expected in both the susceptibility and intensity models (see Appendix 1 for the methodological overview of these models).

Mapping unit choice and dependent and independent variables' assignment

To represent the DF information over space, we chose the slope unit partition of Scotland which can be seen in Fig. 2. A Slope Unit (SU) encompasses the geographic space between streams and ridges (Amato et al. 2019), and a number of analytical tools to extract them from digital elevation models (DEMs) have been developed with time. From the first inception by Carrara et al. (1991), SUs have been manually mapped (Guzzetti et al. 2006) and later obtained via the Inverse DEM method (Turel and Frost 2011). Recently though, a robust computational scheme has been introduced by Alvioli et al.
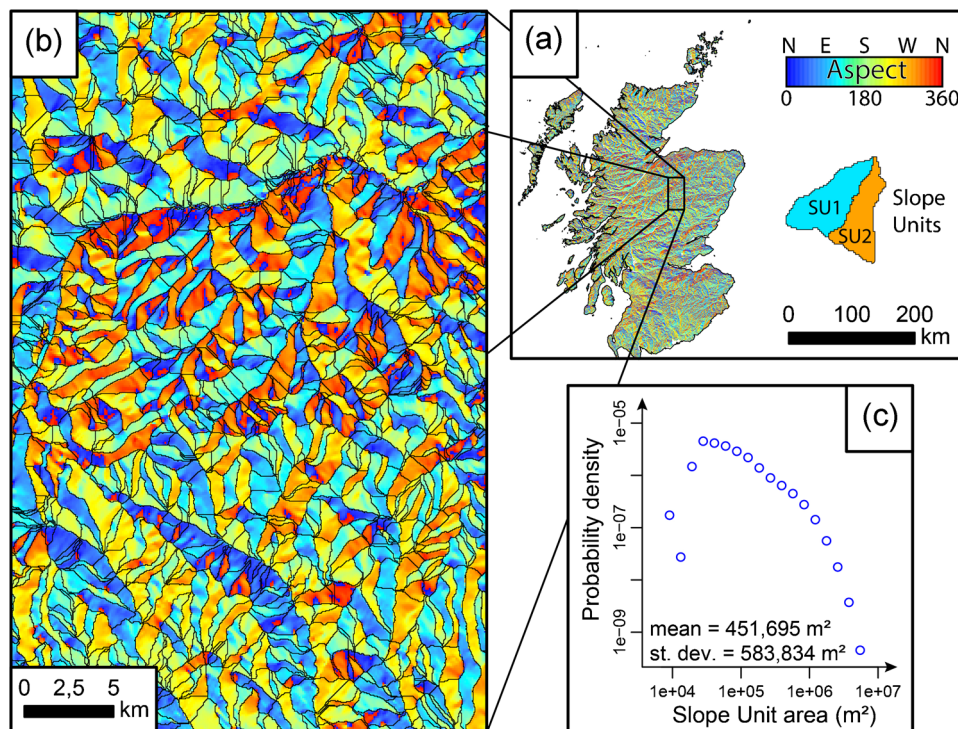
Fig. 2 Panel (**a**): The aspect distribution over the entirety of the Scottish landscape. Panel (**b**): Highlights the slope unit delineation over a small area to provide an overview of the partition and the typical mapping unit sizes. Panel (**c**): The frequency-area distribution of the slope units over the whole Scotland. Notably, the frequency area distributions highlights how dissected the Scottish landscapes is, with an estimated mean SU area, smaller than its standard deviation

(2016) in the form of a GRASS GIS (Neteler and Mitasova 2013) script named *r.slopeunits*. In this work we opted to use *r.slopeunits*, parameterizing it with the following values:

- Flow accumulation threshold = 1,000,000
- Circular variance = 0.3
- Minimum area = 25,000
- Clean size = 10,000

The resulting procedure produced a total of 153,282 SUs, whose geographic overview and frequency area distribution are shown in Fig. 2.

Notably, SUs are irregular polygonal objects whose spatial extent largely exceeds the resolution of common terrain and thematic covariates. For this reason, SUs require an aggregation step to express both dependent and independent variables for each polygon. The dependent one corresponds in our case to the landslide presence and absence, to be assigned at the intersection between landslide identification points and SUs. This aspect concerns the susceptibility model only. In fact, for the LGCP model, the point pattern theoretical foundation requires the locations to be kept with their original details (Bagchi and Illian 2015). The aggregation at the SU level becomes part of the modelling protocol only as a post-processing routine. As for assigning the relevant covariates, the aggregation is performed here by computing the mean and standard deviation within an SU polygon. These are denoted as μ and σ in the suffixes reported in Table 1, where we list all covariates, we opted for to explain the landslide distribution in Scotland. Notably, when we considered the rainfall information, we did not compute the two summary statistics mentioned above because of the coarse resolution of the corresponding precipitation layer (1 km). Moreover, the aggregation of the three different lithological information was performed by computing the predominant class for each SU (Tables 2 and 3).

Method

For reasons of conciseness, a full overview of the proposed methodological protocol is provided in Appendix 1. There, we will introduce a summary of our experimental design, an explanation of Bayesian inference and its connection to Latent Gaussian

Table 1 Summary of the Scotland dataset, including the responses and initial covariates' set

Variable	Acronym	Type	Units	Original scale or resolution	Source
Debris inventory flow	$O_{DF}(s)$	Binary response	0 = absence, 1 = presence	N/A	BGS national landslide database
Debris inventory flow	$Count_{DF}(s)$	Count response	Unit-less	N/A	BGS national landslide database
SU area	SU_A	Continuous explanatory	$m2$	N/A	NextMap DTM (2007); BlueSky (2014/15)
Local relief within 1000-m buffer	LR	Continuous explanatory	m	10 m	Extracted from the DTM
Slope mean and standard deviation	$SLO\ \mu\ and\ \sigma$	Continuous	Degrees	10 m	Extracted from the DTM
Annual precipitation mean and maximum over a 20-year record	$Prec_\mu\ and\ Prec_{max}$	Continuous explanatory	mm	1000 m	MetOffice HadUK-Grid gridded climate observations, (1999–2019)
Profile curvature mean and SD	$PRC\ \mu\ and\ \sigma$	Continuous explanatory	1/m	10 m	Extracted from the DTM
Planform curvature mean and SD	$PLC\ \mu\ and\ \sigma$	Continuous explanatory	1/m	10 m	Extracted from the DTM
Quaternary domain	$Quat$	Categorical explanatory	Unit-less	From 1:10,000 to 1:1,000,000	BGS quaternary domains
Superficial deposit	$Super$	Categorical explanatory	Unit-less	1:625,000	See caption
Bedrock	$Bedrock$	Categorical explanatory	Unit-less	1:625,000	See caption

We stress here that the native DEM resolution is 100 m², obtained by Intermap Technologies (2007). Rainfall data is obtained at this link: https://www.metoffice.gov.uk/ research/climat e/maps-anddata/data/hadu k-grid/datasets. Similarly, the quaternary domain source is https://www.bgs.ac.uk/geology-projects/shallow-geohazards/landslide-domains/; superficial deposits and bedrock were accessed at: https://www.bgs.ac.uk/datasets/bgs-geology-625k-digmapgb/. Planar and profile curvatures have been computed following Heerdegen and Beran (1982)

Table 2 Summary of selected covariates for the susceptibility model (see Appendix 1)

Fixed effects	Random effects	Categorical effects
$SLO\,\sigma$, $Prec_{max}$	LR, $SLO\,\mu$	$Quat$

Table 3 Summary of selected covariates for the LGCP model (see Appendix 1)

Fixed effects	Random effects
$SLO\,\sigma$, $PRC\,\sigma$	$SLO\,\mu$, $Prec_{max}$, LR

Models. This will serve the purpose of clarifying our debris-flow susceptibility and Log-Gaussian Cox process model. As for all the acronyms and terms provided in the manuscript, a summary table is provided in Table 4 of Appendix 2.

Results

This section reports the outcome of our modelling protocol. Due to the dual set of experiments, we have run, the susceptibility and intensity results will be presented separately, first by showcasing the covariate effects, then converting the model estimates into map form.

Susceptibility model

As detailed in Appendix 1, the variable selection procedure isolated a subset of the initial covariates. Their marginal effects are presented in Fig. 3. There, the influence of the local relief (LR) appears as the most dominant covariate among all the selected ones. We recall here that LR is computed as the difference between the maximum and minimum elevation values within a single SU. Therefore, this is commonly interpreted as a proxy for gravitational potential,
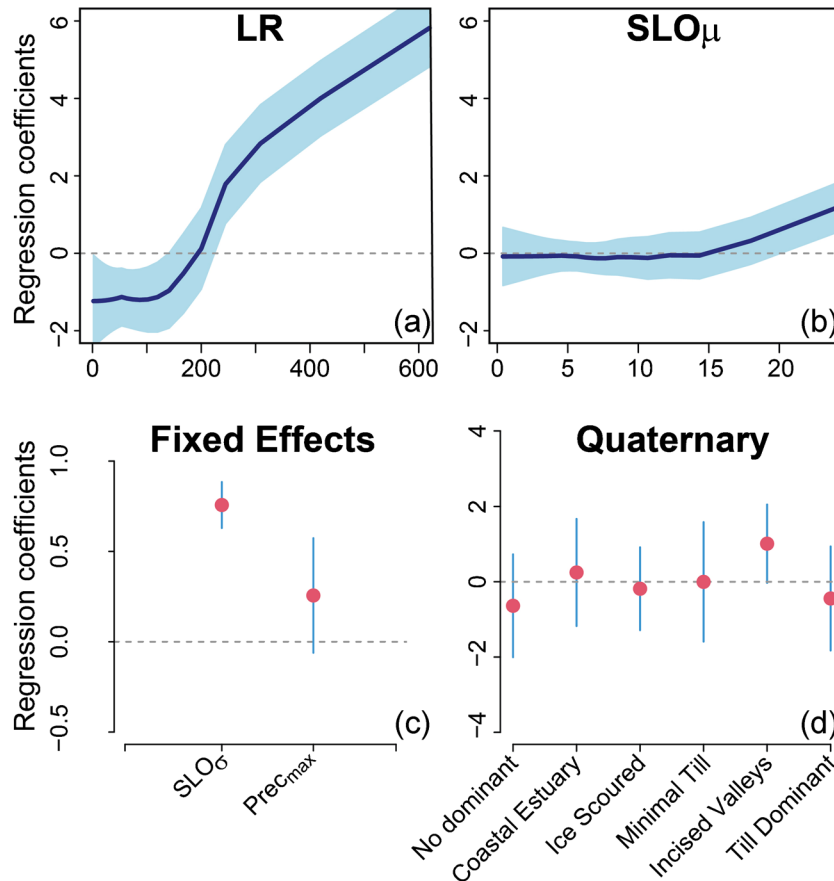
Fig. 3 Posterior means (dark blue curves) of random effects with 95% pointwise credible intervals (light blue shaded area) (top row). Posterior means (dots) of fixed linear effects (except the intercept) with 95% credible intervals (vertical segments) and of categorical quaternary effects (bottom row). The horizontal grey dashed lines indicate no contribution to the DF occurrence. Panels (**a**) and (**b**): Two RW1 effects for local relief and mean slope per SU. Panel (**c**): The standard deviation of the Slope and the maximum Precipitation linear contributions to the model. Panel (**d**): The categorical influence of the quaternary domains

a property intrinsically linked to DF predisposition (see Iverson 1997). Specifically, the inferred pattern points out a negative contribution of the relief up to 200 m. From this elevation difference to approximately 250 m, the LR contribution to the DF occurrence probability rapidly increases and transitions to an approximate linear and positive trend up to 600 m.

Figure 3 additionally highlights the contribution of the average steepness per SU (SLO_μ). We recall here that steepness is also a measure of variation in elevation. The LR estimates differences over a large neighbourhood whereas steepness values are computed as the first order derivative between two adjacent grid-cells. Therefore, the LR and SLO_μ can be considered as the two sides of the same morphometric coin. A closer look at the latter marks a contribution to the susceptibility with a negligible effect up to approximately 15° of mean steepness per slope unit. After which, the trend becomes positive and approximately linear up to the limit of 25°. Interestingly, 21° is empirically referred to by Iverson (1997) as a potential threshold for a slope to become prone to DFs. Moving to the fixed effects, two were selected as such. The first is the SLO_σ, another parameter capable of capturing topographic roughness. Its contribution to the susceptibility model appears positive (mean $\beta_{SLO\sigma}$ = 0.710) and significant (95% of the regression coefficient distribution shares the same sign). A lower and still linear contribution is also estimated for the 20-year maximum rainfall amount computed per SU (mean $\beta_{PRECmax}$ = 0.009). In this case, though, the covariate misses significance by a slight margin, with the 97.5 percentile of the regression coefficient distribution being markedly positive while the 2.5% appears negative. Nevertheless, the mean is still quite far away from the zero-line shown in the plot, thus implying a non-negligible contribution to the model, on average, which is expected for a covariate that should be linked to the DF genetic process. As DF records were not accompanied by their temporal information in the inventory metadata, we could only opt for a general meteorological representation of the Scottish landscape, rather than a precise measure of the trigger pattern in space and time. Ultimately, the bottom-right panel of Fig. 3 presents the categorical effect of the morphology left by the last quaternary glaciation retreat (addressed as Quaternary). Among all the landforms, only the Incised Valleys have been estimated with a positive and significant contribution to the DF occurrence probability. This is geomorphologically sound, and a result commonly retrieved in other DF susceptibility studies tailored to flow-like landslides in Scottish terrains (Ballantyne 1986; Milne et al. 2015). All the remaining quaternary classes, appear not to be statistically significant nor do their regression coefficient appear to be large enough to cause notable variations to the susceptibility pattern, on average.

The sum of all mean susceptibility model components, together with the global intercept and after the logit transformation, produce the estimated susceptibility map shown in the left panel of Fig. 4. Furthermore, the variability estimated for each of the regression coefficients shown in Fig. 3, leads to the uncertainty estimates mapped in the central panel of Fig. 4. What stands out is that the model produces susceptibility patterns for which the central sector of Scotland appears to be largely prone to DFs. Conversely, the southernmost, easternmost and northernmost districts generally present non-susceptible characteristics. However, each of these districts is associated with a different probabilistic pattern when we include uncertainty-oriented considerations. The northern and eastern districts show very low mean susceptibility values

associated with very low uncertainty values. Therefore, this is a portion of the landscape largely to be considered secure from a risk assessment perspective. As for the southern case, low susceptibility values are generally accompanied by high uncertainty levels. In turn, this may indicate a potential danger and require further attention rather than consider this district safe. Making such consideration is crucial and it is also the reason why Bayesian statistics is so widely adopted across virtually any scientific field. However, for a science such as geomorphology intrinsically connected to environmental policies, producing separate maps and commenting on their relative patterns is not ideal. This is the case because traditionally, decisionmakers do not have formal statistical training and, at times, a geoscientific one (Betcherman 1993). Therefore, reading and interpreting the map's probabilistic indication could be difficult. For this reason, here, we propose a simple yet informative alternative to conveying the full probabilistic prediction, in the form of mean values and uncertainty estimates around those. Our approach is to perform a first post-processing step where the mean posterior estimates are binned into a few classes. Here, we choose three for simplicity, to be plotted according to a standard traffic light criterion, corresponding to low (green), medium (yellow) and high (red) susceptibility values. We export all SUs belonging to a given class in a separate file, reporting the width of the 95% credible interval (CI) for each unit. We then plot each file separately, assigning a monochromatic colour bar whose intense colours correspond to SUs with low uncertainty and faded colours for SUs with high uncertainty. By plotting the three files together, we produce a unified probabilistic overview of the model in map form. We believe this to be a solution to a common problem between scientists and policymakers, and further consideration on this topic will be provided in the "Model performance assessment" section.

LGCP

The marginal effects for the variables selected by the procedure mentioned in Appendix 1 are presented in Fig. 5. Interestingly, the selected covariates boil down to those of the same nature selected in the susceptibility case. Specifically, meteorological and terrain characteristics control the variation of the DF intensity. However, the situation for the LGCP model is flipped as compared to the susceptibility one. In fact, the annual rainfall maxima over a period of 20 years appear to be much more closely linked to the response variable and morphometric characteristics that come after it. We recall once more that the intensity of an LGCP model can be considered a rate of DF occurrences in a given neighbourhood. Therefore, the spatial information this parameter conveys is ideally more complex than the simpler binary case tackled in a susceptibility task. This may be partially the reason behind the dominant contribution of rainfall extremes (the maximum among the yearly sums taken over a period of 20 years) towards the intensity. We would like to stress once more something partially referred to in the susceptibility case. Such a rainfall covariate should not be interpreted in the same way as in landslide early warnings (Guzzetti et al. 2020), where the rainfall is measured in a much narrower time window, comparable to the landslide failure process. In fact, the DF inventory we used does not report the landslide date and time of occurrence, therefore hindering the possibility of building temporal or spatiotemporal models. Conversely, the DF data representation we
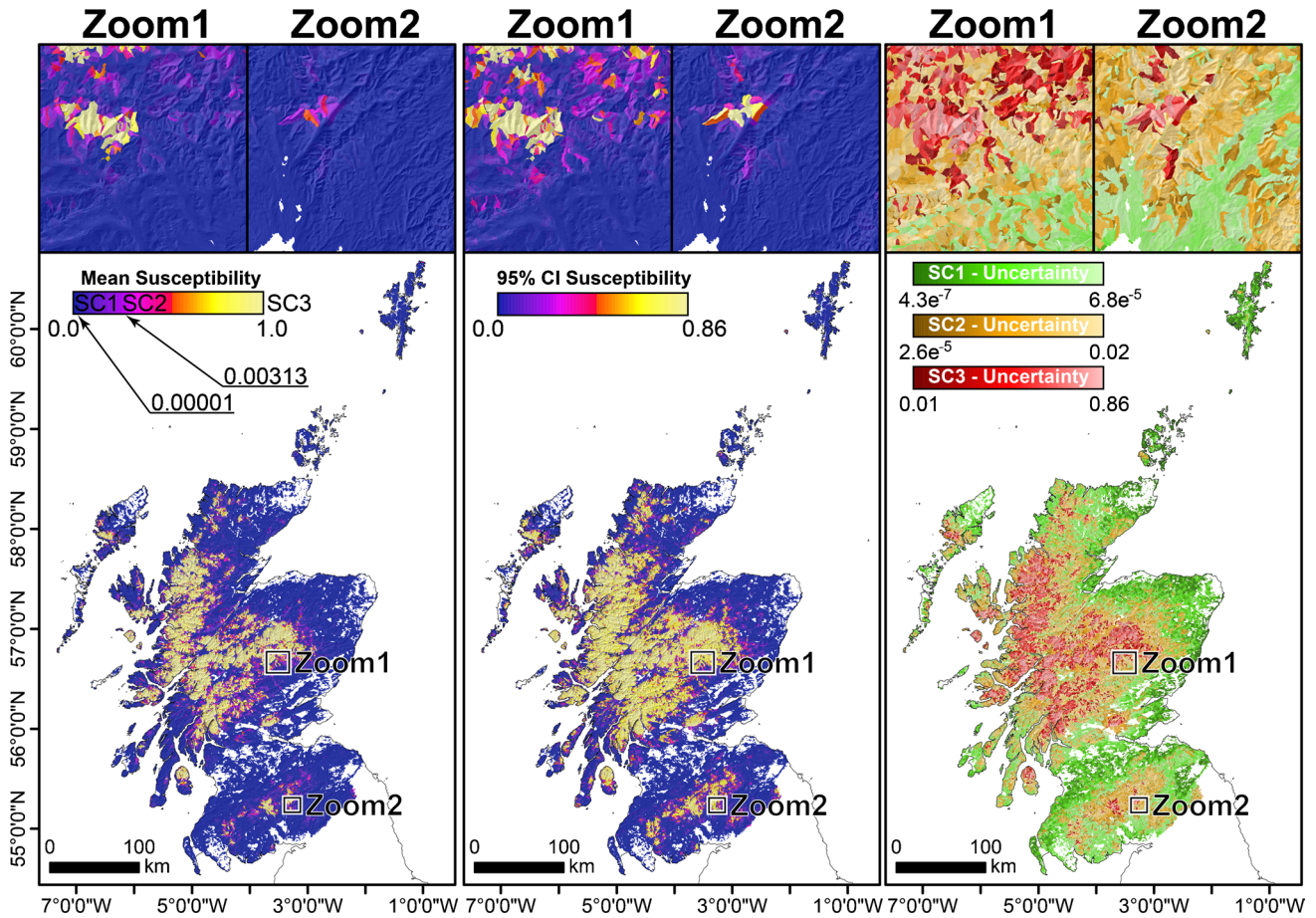
Fig. 4 Mean DF susceptibility based on the presence/absence observations (left), the associated width of 95% CI (middle), and the combined mean susceptibility graded by its uncertainty (right)

use is purely spatial and thus the rainfall interpretation needs to be simplified and summarised to a spatial context only. As a result, the maximum values among the annual accumulated ones over two decades exclusively reflect the geographic tendency of the Scottish landscape to be exposed to intense precipitation. Going back to the estimated effect, the first panel of Fig. 5 highlights a gradual positive trend, distinguishable into two main near-linear segments. The first one starts at an approximate maximum of 1000 mm and continues with a similar incremental rate up to 2100 mm. Up to this point, the contribution still appears to decrease the expected rate of DF occurrences per SU. Conversely, from this point to around 2500 mm the effect shifts to a positive contribution to the estimated DF intensity, after which, it reaches a sort of plateau up to 4,500 mm. The second largest contributor to the landslide intensity appears to be SLO_μ. Differently from the susceptibility case, here the mean SU steepness appears to be much more relevant, behaving according to a marked non-linear trend. This time, the effect is negative overall up to ten degrees, while showing a positive incremental trend that continues until 27°. The third panel of Fig. 5 shows the non-linear effect of linear relief (LR) on DF intensity which, as mentioned before, is a diagnostic of higher energy potential. The effect is negative up to 200 m before increasing its positive effect until a spike at around 250 m. From here, the effect is shortly negative in its

influence before regaining a positive trend until 600 m. The final panel of Fig. 5 shows the linear effects of the standard deviation of the profile curvature and the standard deviation of the slope per SU, with profile curvature being negative ($\beta_{PRC\sigma} = -0.319$) and significant and the latter being positive ($\beta_{SLO\sigma} = 0.520$) and significant. The variation in the profile curvature per slope is something that we can interpret in terms of roughness. In other words, large variations would imply a rough terrain where the curvature measured across the vertical direction changes frequently in a stepped-like manner. Conversely, low variations would imply a relatively smooth surface. For this reason, we interpret a negative regression coefficient as additional topographic information to that carried by SLO_μ. Specifically, SUs with high average steepness values but with the same being largely kept constant across the vertical profile are prone to host large numbers of DFs. A justification for this may be assumed in the geotechnical interpretation of large curvature variations. In fact, mostly hard materials have the capacity to produce stepped-like landscapes, and they are mostly not capable of releasing shallow landslides but rather rockfalls or topples (Frattini and Crosta 2013). As for constant- or near- constant steep slopes, these are diagnostic of soft unconsolidated materials or soils draping over the bedrock. Thus, these are naturally the ideal hosts for DFs (Iverson 1997).
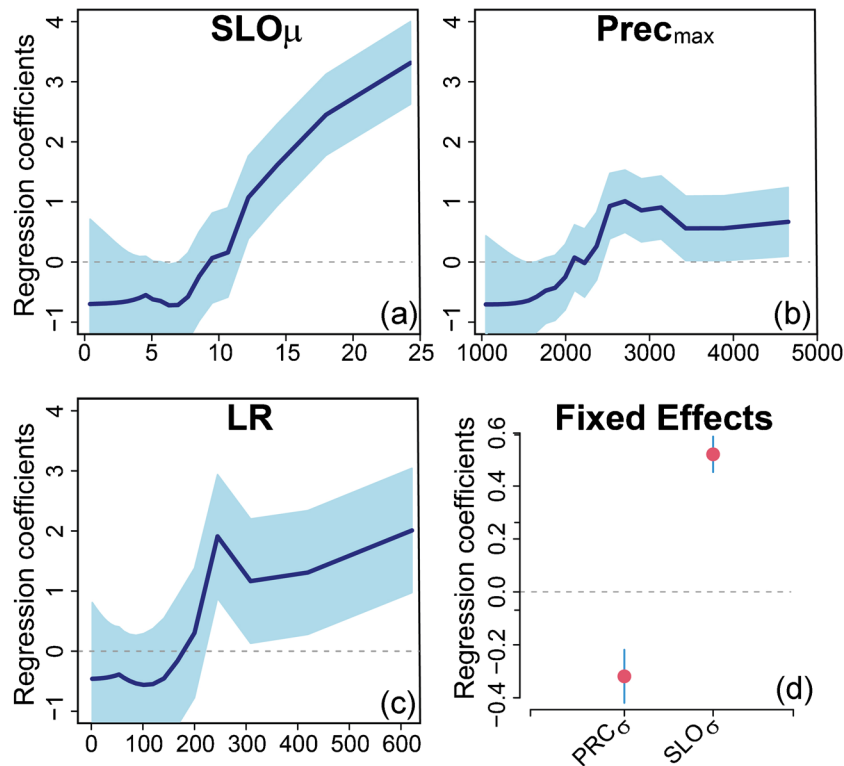
Fig. 5 Posterior means (dark blue curves) of random effects with 95% pointwise CI (light blue shaded area) for the LGCP (panels **a**, **b**, and **c**). Posterior means (dots) of fixed linear effects (except the intercept) with 95% CI (vertical segments) for the LGCP (**d**). The horizontal grey dashed lines indicate no contribution to the DF occurrence. Panels (**a**), (**b**), and (**c**): The RW1 effect carried by the mean slope per SU, the maximum precipitation, and the local relief, respectively. Panel (**d**): The linear contributions to the model of both the standard deviations of profile curvature and slope per SU

Analogously to the susceptibility case, the sum of all mean LGCP model components, together with the global intercept and after the exponential transformation—required to convert the intensity from the log to the linear scale—produce the estimated mean DF intensity map shown in the left panel of Fig. 6. What stands out is that the DF intensity is mostly concentrated on the West coast and central Scotland. Something to be stressed here is that the patterns arising between the susceptibility and the intensity are quite similar. This being said, the information contained in the two maps is not the same. In fact, the susceptibility purely contains information on the occurrence probability whereas the intensity contains information closer to the requirement of hazard modelling. In fact, if we assume a mean DF size (area or volume) then a higher rate of DFs per SU would lead to a higher expected hazard. Conversely, if we consider an average DF size in the context of susceptibility, the associated map will not account for the number of events and therefore to the expected hazard in a given SU. Another interesting element in maps shown in Fig. 6 corresponds to the variability in the mean intensity estimates, shown in the central panel. What we see here is that the variation is minimal. This is comforting information because it generally indicates that the expected intensity or hazard associated with a given SU is robust. As for the last panel, the similarity that characterised susceptibility and intensity in their respective first two maps ceases to hold here. In fact, the pattern of the combined

intensity/uncertainty highlights has less variability than what is shown for the susceptibility. This in turn may indicate that not only the intensity mapping is more informative than its susceptibility counterpart but that the model is also more certain about its output. As a result, an ideal use of such a map may be more effective for decision-makers.

Model performance assessment

In this section, we provide an overview of the performance assessment, spanning over the fitting and cross-validation routines, implemented for the susceptibility and LGCP models, respectively.

The left panel of Fig. 7 shows the goodness-of-fit for the susceptibility case, through a ROC curve with an AUC of 0.97. We recall here that the ROC curve is a measure of the true positive rate (unstable SUs predicted by the model to be unstable, as a fraction of the total number of unstable SUs) against the false positive rate (stable SUs predicted by the model to be unstable, as a fraction of the total number of stable SUs) (Bewick et al. 2004). Such a value is an indication of extremely high explanatory power (outstanding according to the classification proposed by Hosmer et al. 2000). To test whether this is due to overfitting, we implemented a tenfold cross-validation (CV). This procedure involves sub-setting the dataset into ten random portions each one made of 10% of all data. Because the SUs are assigned with a presence/absence label according to the intersection of a debris flow initiation point, the random subsets constitute a
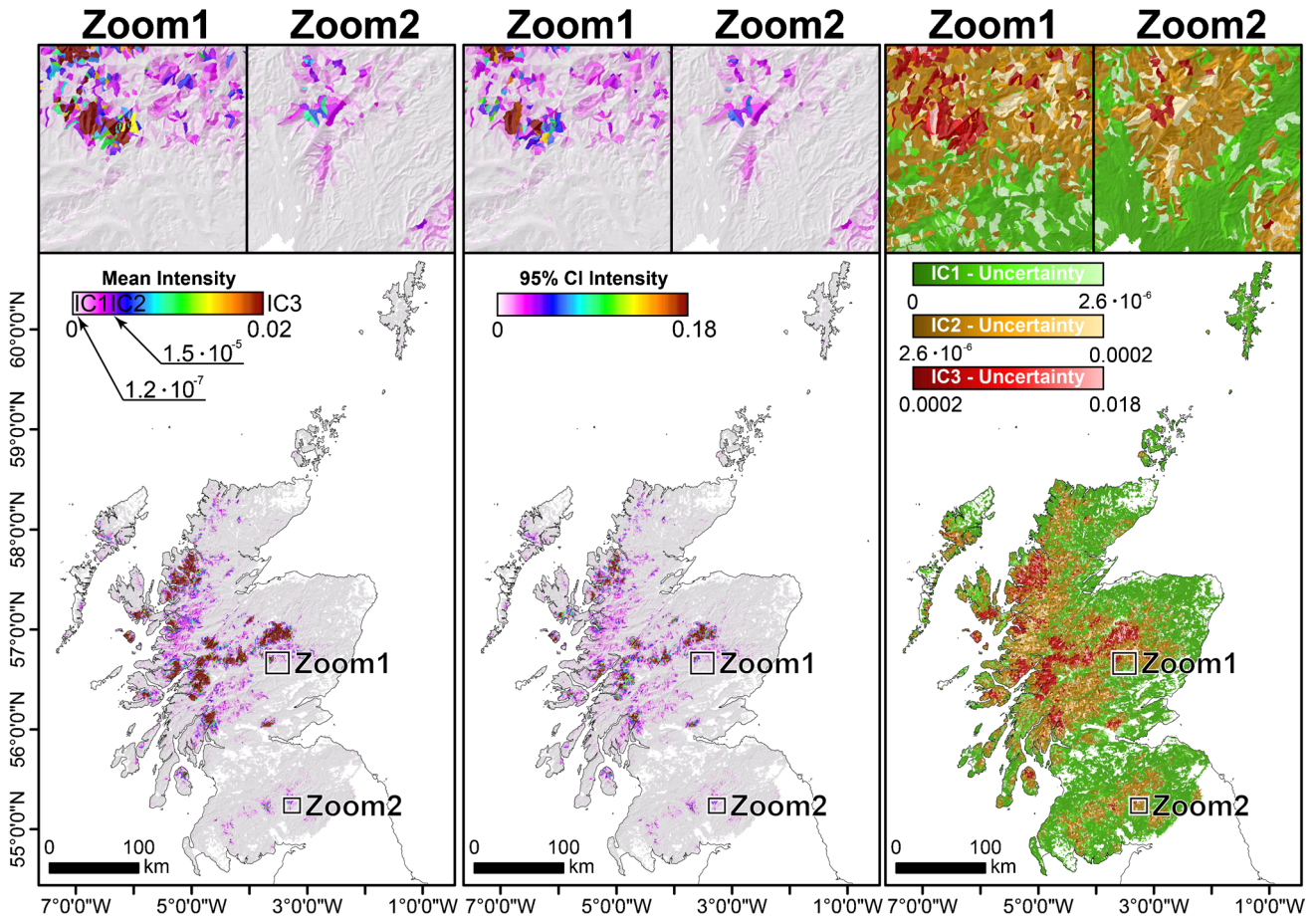
Fig. 6 Mean DF intensity (left), the associated width of 95% credible intervals (middle), and the combined mean intensity graded by its uncertainty (right) aggregated across the Scottish SUs
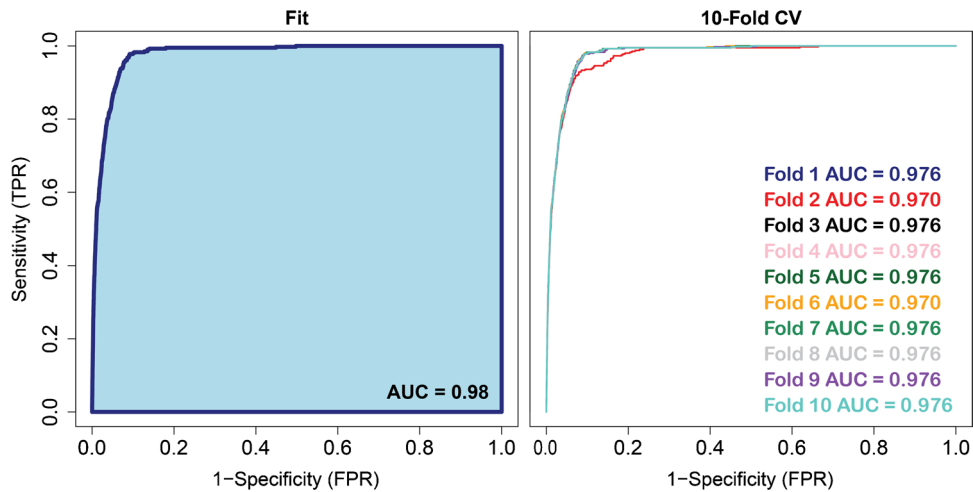
Fig. 7 ROC curve and AUC value for the susceptibility model fit (left panel) and the tenfold cross validation ROC curves and associated AUC values for the susceptibility model (right panel)

smaller version of the initial matrix, with the added constraint that each subset is mutually exclusive from the other nine. As a result, the union of the ten subsets returns the whole Scottish territory. The tenfold prediction skill is graphically shown in the right panel, where the ten receiver operating characteristic (ROC) curves appear to showcase a limited, if not negligible, spread. This attests to the model's robustness. Aside from pure modelling considerations, going back to the susceptibility map, such high predictive power reflects the ability of the model to constraint the unstable labelling to the yellow region highlighted in Fig. 4, where essentially most of the Scottish SUs that host at least one DF takes place.

Validation and model assessment are generally complex for LGCP models as we are interested in points in space rather than some value at said point. However, as we used the Poisson approximation to the LGCP likelihood, we can use the same tenfold cross-validation technique to divide the SUs and examine the DF counts as a function of the model's resulting mean intensity, thus creating an approximation for cross-validation for the LGCP.

Looking at the results of the assessment counterpart for the LGCP, the performance also appears good albeit less outstanding. The left panel of Fig. 8 shows the observed count per SU versus the fitted count per SU, obtained by multiplying the SU mean intensity by the corresponding SU area. The agreement between the two parameters appears to hold for small counts. However, it shows an increasing deviance for large counts. This is most likely because very high counts are much less represented in the model. Therefore, small to medium counts are relatively easy to model because the LGCP learns from the available data. As for the medium to high counts, their small numbers hinder the ability of the LGCP to reflect them in the fitted results.

The prediction skill of the LGCP is presented in the right panel of Fig. 8, where the observed counts are plotted against their predicted counterparts in the same tenfold division manner as the susceptibility case. The plot shows a similar behaviour as compared to the fit, with low to medium counts being suitably estimated. However, the prediction of medium to high counts is not as good. This attests once

more to the model robustness, where little variations are experienced at changing the modelled data. Similar to the susceptibility case, if we look at the locations where high mean DF intensity is shown in Fig. 6, a high predictive power means that the region from SW to NE where high DF rates per SU are observed is consistently recognized.

Discussion

Binary vs count based modelling reflections

Here we reflect on the noticeable effects of using one modelling procedure (susceptibility case) and the other (intensity case). The susceptibility model produced exceptionally high goodness-of-fit and predictive performance diagnostics (see Fig. 7). When we first observed the outstanding classification (Hosmer et al. 2000) in the left panel, we assumed it to be potentially due to some clustering or spatial structure within the covariates. If that were the case, implementing a spatial cross-validation routine would have been capable of breaking down or reducing the contribution of any spatial structure, thus producing spatially unbiased predictive performances. As a result, we would have also noticed a marked decrease in the estimated classification metrics. However, the right panel still shows outstanding predictions. For this reason, we further investigated whether this could be due to some potentially biased covariates, as per Steger et al. (2021). To do so we circled back and generated five single-variable models, one for each covariate selected in our benchmark susceptibility. Interestingly, extremely high performance is obtained solely using LR or SLO_μ. These are not covariates that should be sensitive to any mapping criterion. In other words, when looking for biasing covariates, one should expect a property to explain a large portion of the DF distribution, this being the case because the covariate itself may be sensitive to the way local geological surveys are carried out to report landslides. For instance, Moreno et al. (2024) found that the effectively surveyed area (a layer expressing proximity to road networks) correlates well with the presence/absence of landslide data in South Tyrol (Italy), a bias they removed from
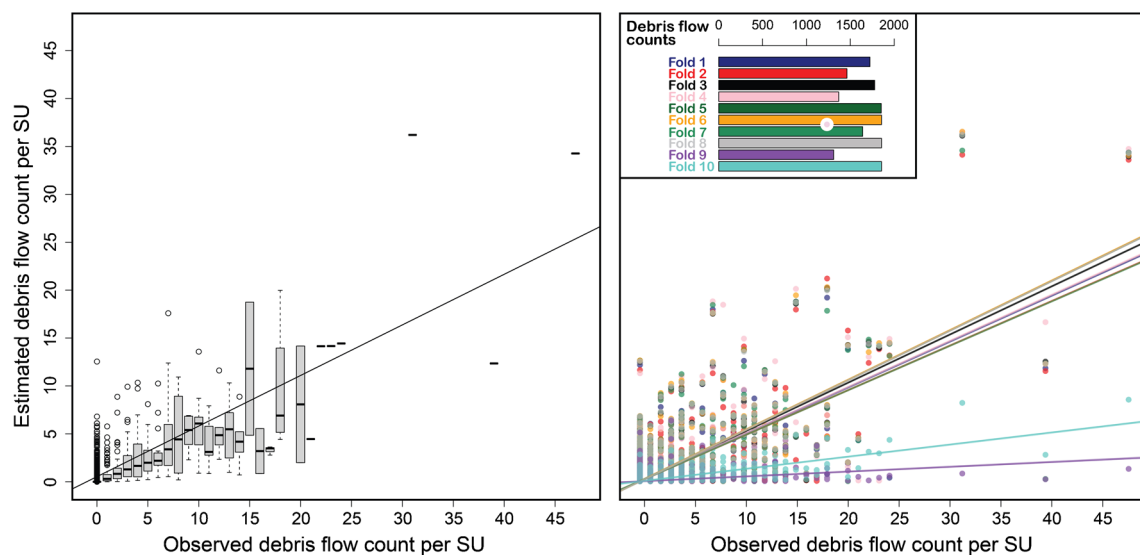
Fig. 8 Observed versus fitted counts for LGCP model (left panel) and observed versus tenfold predicted counts for LGCP model (right panel)

the model by zeroing out the associated regression coefficient. In our case, we have no reason to assume that the inclusion of the LR and SLO_μ is closely associated with any mapping practice behind the Scottish DF inventory. Despite that this is an uncommon result, we believe our model to be reliable and the effect of these two terrain characteristics to be realistic. We support this argument by benchmarking our model against the GeoSure model, and by comparing the covariate effects estimated as part of the intensity procedure. Analogous susceptibility patterns can in fact be seen also in the GeoSure map (Fig. 9b). At the time of the GeoSure heuristic development most of the DFs we used were not available, especially those that have been mapped in response to public notice. Therefore, it is highly unlikely that the public would report DFs, depending on the terrain arrangement and it is rather more reasonable to assume that the slope geometry may largely contribute to the genesis of DF in Scotland. An additional

verification can be seen in the intensity model. There, a more reasonable performance is obtained, far from being outstanding. This actually brings another point of discussion. After many years of data-driven methodological development, outstanding performances have become commonplace among many susceptibility contributions. For instance, outstanding performance diagnostics, e.g. AUC > 0.95, are nowadays reported frequently in a number of articles adopting advanced spatial statistics (Lombardo et al. 2020a, b), machine (Di Napoli et al. 2020) and deep (Lv et al. 2022) learning. Therefore, the point we are trying to raise here is questioning whether the susceptibility framework shouldn't be considered largely solved (Ozturk et al. 2021), whenever heavily non-linear models are tasked with distinguishing the distribution of landslides purely in space. Conversely, the data-driven estimation of landslide intensity (Lari et al. 2014), whether it is spatially (Moreno et al. 2023), temporally (Nava et al. 2023),
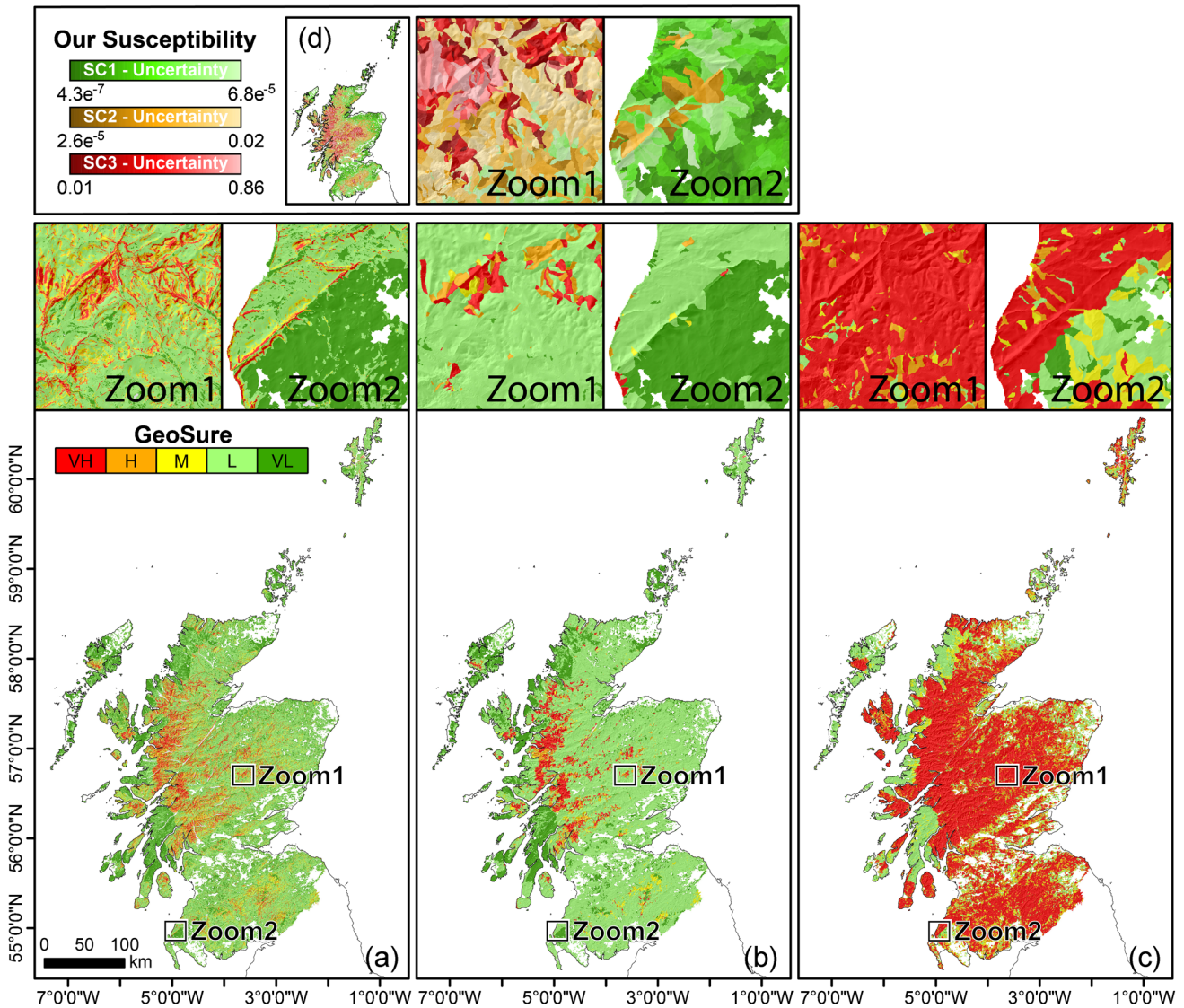
Fig. 9 GeoSure DF susceptibility (**a**), aggregated on the basis of a majority criterion per SU (**b**), and according to the highest class per SU (**c**). Panel (**d**): A reduced version of the DF susceptibility built in this work and already mapped in Fig. 4

or spatiotemporally (Fang et al. 2024) addressed it is still at an infancy stage where few contributions are available and much may still be gained from a common geoscientific effort.

GeoSure benchmark

In this Section, we opted to compare the GeoSure DF susceptibility layer against the DF susceptibility we produced here. Figure 9 allows for such comparison by reporting in Fig. 9a, the original GeoSure raster at 50 m resolution. Because our model is expressed at the SU scale, we opted to aggregate the 50 m information over SUs, following two separate criteria: the first (Fig. 9b) assigns the most frequent DF susceptibility class while the second (Fig. 9c) assigns the worst case scenario. In other words, the first criterion calculates how many 50-m pixels fall among the five GeoSure categories (VL = very low, L = Low, M = medium, H = high, VH = very high), and assigns to each slope unit the most representative class. The second approach assigns the highest class, irrespective of its numerosity per SU. We recall here that the definition of susceptibility refers to the probability of having at least one landslide occur. For this reason, we also included the second approach, to account for at least one high probability pixel.

What immediately stands out is that the probability patterns of our mean DF susceptibility and the pixel-based GeoSure largely match across Scotland. The same consideration applies when looking at the GeoSure majority aggregation per SU, but it is not the case for the GeoSure worst-case scenario.

As for the match at the local level, GeoSure tends to polarise the susceptibility estimates either in the VL to L classes or in the H to VH class, leaving the intermediate class less represented. This is mostly an effect due to the expert-based structure behind the current GeoSure maps and it becomes particularly evident in the Zoom1 of Fig. 9a, where the effect of the slope steepness map largely controls the susceptibility classes, with no other apparent contribution coming from other predictors.

The same is true for Zoom2 of the same panel. There, the effect of a geological type that has received a negative weight flattens out the susceptibility, which mostly falls in the VL category. By comparison, our mean DF susceptibility provides a richer description of the process, not only because it includes the uncertainty, but also because its patterns appear more realistic.

Another interesting element to consider has to do with the pixel structure of a susceptibility map, and this reasoning goes well beyond the specific case and rather applies to any similar gridded map versus an SU-based one. In fact, if one selects grids as the mapping unit of choice, the most common effect is to obtain "salt and pepper" looking maps. This is again visible in Fig. 9a, where the zooms highlight single pixels falling in the VH susceptibility class being entirely surrounded by pixels falling in the L or even VL classes. This constitutes a problem for decision-makers because slope stabilisation practices cannot be applied to single grid cells but rather to the whole slope they belong to. This "salt and pepper" effect propagates to the susceptibility in Fig. 9c. Risk-oriented applications are often tailored towards worst-case scenarios and here what becomes evident is that almost every SU in Scotland hosts at least one VH susceptibility pixel. However, not every slope in Scotland fails and luckily so, which in turn points to the limited realistic representation of a landscape in grid-based models.

General considerations and future improvements

In this section, we review the two models presented, look at their possible limitations and suggest future improvements.

Firstly, we note that the data is as complete and representative as possible. Therefore, modelling the higher DF counts is unlikely to be improved with this methodology as there is no way to gain more data on higher counts if none exist. However, we can extend the data framework to account for a larger domain—the whole of GB for example—and in this way, we can gather more information on the spread of DF count and its dependence on the covariate set we chose.

Secondly, the covariate information and the modelling methodology are purely spatial. This is an informative start, but extending the point process modelling towards spatiotemporal structures could explain varying patterns of DF intensity. However, some degree of variations to the model should be implemented. For instance, the covariates should be revisited. Presently, we used an aggregate of the maximum daily precipitation over a 20-year period, calculating averages on an annual basis. Rainfall has a high correlation with DF intensity but with a spatial model, we can only account for one statistic (the average of the maxima) to describe the whole rainfall pattern. If we used a spatiotemporal LGCP model, we could use a function to describe the pattern of rainfall over a period of time that might influence the slope instability—prior and past to the DF event. This would improve prediction ability and provide a model that is interpretable over time. In turn, this could open up towards a new generation of early warning systems for Scottish debris flows. However, it should be stressed that not all the data points we used have an associated date and ideally we would want the complete data. The geoscientific community is working hard to improve this, mainly in the form of automated mapping procedures, thanks to the high orbital frequency modern satellites offer.

Overall, the DF susceptibility and DF intensity maps both capture the areas in which to focus in terms of a higher DF risk. The LGCP model intensity map however, perhaps pinpoints these areas with a higher degree of accuracy due to the nature of the point process modelling approach. Both models do well in terms of model performance, although validation measures for point-process models are generally complex and more along the lines of a residual analysis to compare variations of the model. Using the DF count per SU allowed us to implement the same tenfold CV scheme that was used to validate the susceptibility model. An improvement here could be conducting a leave-one-group-out cross-validation (Liu and Rue 2022). When one SU is removed, the underlying spatial correlation between SUs can still be closely approximated by the surrounding SUs. Removing a group of SUs at a time would better test the model's prediction abilities by accounting for the absence of this spatial correlation when a group of SUs are removed.

A final improvement to the model can be achieved with the integration of information from the BGS National Geotechnical Database (British Geological Survey National Geotechnical Database 2019) on the geographical distribution of physical properties of a wide range of rocks and soils present in GB. Presently, the information is relatively coarse across space which makes its integration into the model difficult at this time. BGS is continuously updating its records and databases which in the future could be used in a model for DF prediction.

We conclude the discussion by pointing out an interesting aspect of the landslide predictive patterns coming from our susceptibility and intensity models, as well as the susceptibility produced for the GeoSure system. The general patterns of the three corresponding maps look similar at a broad examination. The main areas where landslides are expected follow two trends, one North to South on the West coast, and another one South-West to North-East starting from the West coast and extending across the central belt. This is interesting because both our models rely on underlying spatial effects whereas the GeoSure map is purely driven by an expert-based weighting system informed by knowledge of the debris flow initiation process.

Conclusions

In this work, we proposed modelling DF occurrence across Scotland using a dual approach that respected the traditional susceptibility requirements as well as a more complex structure that extended the estimation towards DF counts per mapping units. In the first case, we opted for a.

Bernoulli distribution model in the Bayesian framework, where we included covariates as fixed and random effects. The count extension is here introduced as a complementary source of information, providing both where and how many events should be expected for specific areas. Such a model is a step forward in the existing LSM of Scotland, developed to provide local stakeholders (local authorities and railway/roadway managers) an overview of debris flow susceptibility across their network and to assist homeowners and developers in reducing social and economic losses. The present contribution aligns well with the activities undertaken by the Natural Hazard Partnership which the BGS supports through its Daily Landslide Hazard Assessment. If a model could be extended to account for spatiotemporal variations in precipitation regimes and associated debris-flow occurrences it could be integrated into the existing forecasting tool used by the BGS to assess rainfall-triggered landslides, however, this requires further data homogenization efforts.

Appendix 1. Methodological overview

We implemented two modelling archetypes: to model landslide susceptibility as per international standards, we can predict the probability of observing at least one DF in a SU by using a Bernoulli distribution (see, Section 4.3). For the LGCP, we model the DF rate of occurrence per SU by using a Poisson distribution with a random intensity function (see Section 4.4) that approximates the LGCP likelihood of the landslide points distributed across the space. In both cases, we can assume that the observations (presence/absence in the susceptibility case or counts in the LGCP case) are conditionally independent given a latent Gaussian process (more details in Section 4.2), where these models can flexibly capture local correlation structure and uncertainty. As a result, the covariates can be modelled flexibly in terms of their influence on DF occurrence or intensity and in the remainder of the manuscript they will be addressed as fixed and random effects to refer to their linear and nonlinear use, respectively. This nomenclature stems from the Bayesian statistical community, and it will be adopted here due to the Bayesian modelling choice we have made (more details in Section 4.1).

Bayesian inference

Bayesian statistics is an approach to data analysis centred on Bayes' theorem. It updates our understanding of model parameters by combining prior knowledge (or prior distribution) with observed data through a likelihood function, yielding a conditional probability known as a posterior distribution. This posterior represents our refined belief about the parameters and can be used to predict future events. Here, we briefly define the three terms mentioned above, namely, conditional probability, likelihood, and prior distribution, in the context of landslide science, and refer the reader to Rue et al. (2017) for further explanation.

Conditional probability refers to the probability of an event occurring given that something else (a set of conditions) is true. In our context, a conditional probability of interest is, e.g., that of an SU being unstable given that the slope is steeper than a certain angle while accounting for other similar geomorphological influencing factors, hereafter referred to as covariates or predictors. The likelihood indicates how likely a population is to produce the observed sample. Using our previous example, it translates into the joint probability of observing an unstable SU computed as a function of the parameters of a statistical model. Finally, a prior distribution represents the best guess about the true value of a model parameter, expressed as a probability distribution. In a regression context with a single regression coefficient, a prior over the coefficient can be interpreted as the initial range of regression coefficients, which will be later updated with the sample information using the Bayes theorem.

Posterior distributions usually involve the calculation of high-dimensional integrals without a closed-form expression. A classical way to approximate these integrals is through Markov chain Monte Carlo (MCMC), which refers to a class of simulation-based methods to create samples from the posterior distributions of interest based on classical convergence results for Markov chains. In practice, MCMC entails tedious and complex computations. These challenges are exacerbated due to the slow or lack of convergence of the chain. A popular alternative was proposed by Martino and Rue (2009) which is the integrated nested Laplace approximation (INLA), a method that approximates posterior distributions in a computationally efficient way by combining Laplace approximation of probabilities with numerical methods using a variational Bayes correction (Van Niekerk 2023). INLA is conveniently accessible via the R-INLA package (Bivand et al. 2015). Due to its computational efficiency, INLA is particularly suitable for incorporating various covariates with different types of effects over the response, including spatial effects with complex dependence structures. Readily available in INLA is the stochastic partial differential equation (SPDE; Lindgren and Rue 2015) approach to approximate Matérn covariance structures between locations. Its importance in our modelling strategy lies in the ability to retrieve unaccounted-for but spatially structured effects over the response (Lombardo et al. 2019).

Gaussian latent models

INLA is constructed for the class of latent Gaussian models (LGMs), a very flexible class of models often used for spatial data (Rue et al. 2017). They have a hierarchical representation where observations

are assumed to be conditionally independent given a latent field and a set of hyperparameters (the reader can refer to Bryce et al. (2022) for a formulation of the hierarchical representation of the latent Gaussian field in the context of landslide modelling). Here, we denote the observations as (s), $s \in \mathcal{S}$ ($\mathcal{S}$ is the study domain; i.e., the collection of SUs), which are assumed to depend on the sum of model components, (s). Our sum of model components has an additive structure, obtained by combining fixed and random effects, together with a term that accounts for the spatial effect among SUs. This is particularly relevant because, in the absence of a spatial effect, SUs located next to each other would be treated exactly in the same way as SUs far apart. As a result, our generic model structure takes the form:

$$\eta(s) = \alpha + \sum M_{m=1} \beta_m w_m(s) + \sum_k K_{=1} f_k(z_k(s)) + u(s), \ s \in \mathcal{S} \qquad (1)$$

where α is an intercept and $(w_1(s),..., (w_M(s))^T$ are a subset of the covariates detailed in Table 1 with fixed (or linear) coefficients $\beta = (\beta_1,..., \beta_M)^T$. The functions $f = \{(\cdot),..., f_K(\cdot)\}$ are random (or non-linear) effects defined in terms of a set of covariates $(z_1(s),..., z_K(s))^T$. The specific form of the functions $(\cdot)$ is that of a Gaussian random walk of order 1 (RW1), defined over a binned version of the covariates. This is used to capture the non-linear relationship the covariate might have with the DF susceptibility or intensity. Lastly, the term (s) is the spatial effect represented by a Gaussian process with Matérn covariance structure. For more details, we refer the reader to Bakka et al. (2018). Overall, the model structure described above is valid both for susceptibility and LGCP cases, denoted as $\eta_{Bernoulli}(s)$ and $\eta_{LGCP}(s)$, and the next two sections will dive into the specifics of how each of the two selected models will tackle the landslide prediction.

The susceptibility model

We model DF susceptibility with a Bernoulli distribution, thus we have that $y(s) = O_{DF}(s) \in \{0,1\}$ and $y(s) \mid \eta_{Bernoulli}(s) \equiv Bernoulli(p(s))$, where $p(s) = Pr\{O_{DF}(s) = 1\}$. The probability.

(s) is related to the sum of model components, $\eta_{Bernoull}(s)$, through the logit link, so that $p(s) = exp\{\eta Bernoulli(s)\} / (1 + exp\{\eta Bernoulli(s)\})$.

The sum of the susceptibility model components, $\eta_{Bernoul}(s)$, follows the general model structure of Eq. 1, with its specific form depending on the influence of the covariates on the DF susceptibility. To find the most appropriate way to express the influence of each covariate, as well as whether each given covariate provides useful information to the model, we conduct a dual-stepped variable selection. This is performed by testing each covariate in a linear and nonlinear form, as well as introducing these two realisations as part of a standard stepwise forward procedure (Steyerberg et al. 1999). This procedure calculates the Deviance Information Criterion and the Watanabe-Akaike Information Criterion (DIC and WAIC respectively; Meyer 2014; Gelman et al. 2014). Out of all the covariates listed in Table 1, the selected ones and their specific form as part of the susceptibility model are detailed below in Table 2 (all the pre-processing is unreported for reasons of conciseness).

The log-Gaussian Cox process

We model the spatial rate of DF occurrences per SU (DF intensity) via a log-Gaussian Cox process (LGCP). This model has a doubly stochastic nature consisting of an inhomogeneous Poisson point process whose random intensity surface is expressed in the logarithmic scale, allowing it to be modelled with a Gaussian likelihood (Illian et al. 2008).

One of the properties of the Poisson distribution is that it is consistent across any spatial resolution due to Poisson additivity. In other words, the sum of N-independent Poisson variables with mean λ_i, $i = 1,..., N$ is again a Poisson variable with mean $\sum_i^N \lambda_i$. From this, we can define a spatial Poisson process over a continuous space such that for example a region, A, within the study area contains a random number of events (e.g., landslides) that follow the Poisson distribution with mean $\lambda(A) = \int_A \lambda(s)$, where $\lambda(s) > 0$ denotes the intensity at location s.

A spatial Poisson process with a spatially varying random intensity $\Lambda(\mathcal{S})$ is called a Cox process and if $\Lambda(\mathcal{S})$ is modelled as a Gaussian process in the log scale, it is known in the statistical literature as an LGCP (Bachl et al. 2019). In the context of latent Gaussian models, $\Lambda(\mathcal{S})$ is linked to the sum of the model components of the same form as Eq. (1) as follows:

$$\Lambda(\mathcal{S}) = exp(\eta(\mathcal{S})) \qquad (2)$$

$$log(\Lambda(\mathcal{S})) = \eta(\mathcal{S}) \qquad (3)$$

A methodology proposed by Illian et al. (2012) allows us to fit an LGCP model using the integrated nested Laplace approximation by constructing a Poisson approximation to the LGCP likelihood. The number of DF points in each cell (defined from a regular lattice over the study area) are counted, $Count_{DF}(s)$, and if we assume that the regular lattice is small enough and that the latent field is correctly discretized then the approximation is sufficient for the LGCP likelihood. In this study, rather than a regular lattice defined, we use the SU partition. This can be further broken down as the number of points in each SU following a Poisson distribution with its mean represented by the intensity of the cell. This intensity is then approximately equal to the area of each cell multiplied by the exponential value of the latent field in each cell.

This process ensures that the number of DFs occurring in an SU can be considered rather than simplified into the binary classification typical of susceptibility studies. In other words, the susceptibility case keeps the zeroes exactly in the same form as the LGCP. However, the positive value is compressed to one, denoting slope instability. Conversely, the LGCP framework allows modelling the numerosity of the slope failures rather than being limited to the presence/absence situation. The selected covariates and their specific form of entry underwent the same variable selection procedure described in Section 4.3. Out of all the covariates listed in Table 1, the selected ones and their specific form as part of the LGCP model are detailed below in Table 3 (all the pre-processing is unreported for reasons of conciseness).

Appendix 2

Please see Table 4.

Table 4 Acronym summary

Full description	Acronym
Landslide susceptibility maps	LSM
British geological survey	BGS
National landslide database	NLD
Log-Gaussian Cox process	LGCP
Integrated nested Laplace approximation	INLA
Stochastic partial differential equation	SPDE
Debris flow	DF
Slope unit	SU
Markov chain Monte Carlo	MCMC
Latent Gaussian models	LGMs
Random walk of order 1	RW1
μ	Mean covariate value in a SU
σ	Mean covariate value in a SU

Declarations

Competing interests The authors declare no competing interests.

References

Alvioli M, Marchesini I, Reichenbach P, Rossi M, Ardizzone F, Fiorucci F, Guzzetti F (2016) Automatic delineation of geomorphological slope units with r. slopeunits v1. 0 and their optimization for landslide susceptibility modeling. Geosci Model Dev 9(11):3975–3991

Amato G, Eisank C, Castro-Camilo D, Lombardo L (2019) Accounting for covariate distributions in slope-unit-based landslide susceptibility models. A case study in the alpine environment. Eng Geol 260:105237. https://doi.org/10.1016/j.enggeo.2019.105237

Atkinson PM, Massari R (1998) Generalised linear modelling of susceptibility to landsliding in the central Apennines, Italy. Comput Geosci 24(4):373–385

Azarafza M, Azarafza M, Akgün H, Atkinson PM, Derakhshani R (2021) Deep learning-based landslide susceptibility mapping. Sci Rep 11(1):24112

Bachl FE, Lindgren F, Borchers DL, Illian JB (2019) inlabru: an R package for Bayesian spatial modelling from ecological survey data. Methods Ecol Evol 10(6):760–766

Bagchi R, Illian JB (2015) A method for analysing replicated point patterns in ecology. Methods Ecol Evol 6(4):482–490

Bakka H, Rue H, Fuglstad GA, Riebler A, Bolin D, Illian J, Krainski E, Simpson D, Lindgren F (2018) Spatial modeling with R-INLA: a review. Wiley Interdiscip Rev: Comput Stat 10(6):e1443

Ballantyne CK (1986) Landslides and slope failures in Scotland: a review. Scott Geogr Mag 102(3):134–150

Betcherman G (1993) Research gaps facing training policy-makers. Canadian public policy/analyse de politiques, pp.18–28. https://doi.org/10.2307/3551787

Bewick V, Cheek L, Ball J (2004) Statistics review 13: receiver operating characteristic curves. Crit Care 8(6):1–5

Bhuyan K, Meena SR, Nava L, van Westen C, Floris M, Catani F (2023) Mapping landslides through a temporal lens: an insight toward multi-temporal landslide mapping using the u-net deep learning model. Gisci Remote Sens 60(1):2182057

Bivand R, Gómez-Rubio V, Rue,H (2015) Spatial data analysis with R-INLA with some extensions. American Statistical Association. https://doi.org/10.18637/jss.v063.i20

BGS National Landslide database (2012) British Geological Survey. Available at: https://www.bgs.ac.uk/datasets/national-landslide-database/. Accessed 17 Sept 2024

National Geotechnical Properties Database (2019) British Geological Survey. Available at: https://www.bgs.ac.uk/geological-research/science-facilities/engineering-geotechnical-capability/nationalgeotechnical-properties-database/. Accessed 17 Sept 2024

BGS Geosure (2019) British Geological Survey. Available at: https://www.bgs.ac.uk/datasets/geosure/. Accessed 17 Sept 2024

GeoClimate UKCP09 and UKCP18 (2022) British Geological Survey. Available at: https://www.bgs.ac.uk/datasets/geoclimate-ukcp09-and-ukcp18/. Accessed 17 Sept 2024

Ciurean R, Lee K (2022) User guide: BGS debris flow susceptibility model for Great Britain (version 6.1), NERC Open Research Archive. Available at: https://nora.nerc.ac.uk/id/eprint/532944. Accessed 17 Sept 2024

Bryce E, Lombardo L, van Westen C, Tanyas H, Castro-Camilo D (2022) Unified landslide hazard assessment using hurdle models: a case study in the Island of Dominica. Stoch Env Res Risk Assess 36(8):2071–2084

Budimir MEA, Atkinson PM, Lewis HG (2015) A systematic review of landslide probability mapping using logistic regression. Landslides 12:419–436

Cama M, Lombardo L, Conoscenti C, Agnesi V, Rotigliano E (2015) Predicting storm-triggered debris flow events: application to the 2009 Ionian Peloritan disaster (Sicily, Italy). Nat Hazards Earth Syst Sci 15(8):1785–1806

Carrara A, Cardinali M, Detti R, Guzzetti F, Pasqui V, Reichenbach P (1991) GIS techniques and statistical models in evaluating landslide hazard. Earth Surf Process Landf 16(5):427–445

Castro-Camilo D, Huser R, Rue H (2019) A spliced gamma-generalized Pareto model for shortterm extreme wind speed probabilistic forecasting. J Agric Biol Environ Stat 24(3):517–534

Castro-Camilo D, Mhalla L, Opitz T (2021) Bayesian space-time gap filling for inference on extreme hot-spots: an application to Red Sea surface temperatures. Extremes 24:105–128

Chang JM, Chen H, Jou BJD, Tsou NC, Lin GW (2017) Characteristics of rainfall intensity, duration, and kinetic energy for landslide triggering in Taiwan. Eng Geol 231:81–87

Chang Z, Huang J, Huang F, Bhuyan K, Meena SR, Catani F (2023) Uncertainty analysis of non-landslide sample selection in landslide susceptibility prediction using slope unit-based machine learning models. Gondwana Res 117:307–320

Cigna F, Bateson LB, Jordan CJ, Dashwood C (2014) Simulating SAR geometric distortions and predicting persistent scatterer densities for ERS-1/2 and ENVISAT C-band SAR and InSAR applications: nationwide feasibility assessment to monitor the landmass of Great Britain with SAR imagery. Remote Sens Environ 152:441–466. https://doi.org/10.1016/j.rse.2014.06.025

Corine Land Cover (2018) (vector/raster 100 m), Europe, 6-yearly (no date) - Copernicus Land Monitoring Service. Available at: https://land.copernicus.eu/en/products/corine-land-cover/clc2018. Accessed 17 Sept 2024

Crozier MJ (2005) Multiple-occurrence regional landslide events in New Zealand: hazard management issues. Landslides 2(4):247–256

Cuevas-Pacheco F, Møller J (2018) Log Gaussian Cox processes on the sphere. Spat Stat 26:69–82

Di Napoli M, Carotenuto F, Cevasco A, Confuorto P, Di Martire D, Firpo M, Pepe G, Raso E, Calcaterra D (2020) Machine learning ensemble modelling as a tool to improve landslide susceptibility mapping reliability. Landslides 17(8):1897–1914

Dong A, Dou J, Fu Y, Zhang R, Xing K (2023) Unraveling the evolution of landslide susceptibility: a systematic review of 30-years of strategic themes and trends. Geocarto Int 38(1):2256308

Fang Z, Wang Y, van Westen C, Lombardo L (2024) Landslide hazard spatiotemporal prediction based on data-driven models: estimating where, when and how large landslide may be. Int J Appl Earth Obs Geoinf 126:103631

Fayne JV, Ahamed A, Roberts-Pierel J, Rumsey AC, Kirschbaum DB (2019) Automated satellite-based landslide identification product for Nepal. Earth Interact 23(3):23–21. https://doi.org/10.1175/EI-D-17-0022.1

Fell R, Corominas J, Bonnard C, Cascini L, Leroi E, Savage WZ (2008) Guidelines for landslide susceptibility, hazard and risk zoning for land use planning. Eng Geol 102(3–4):85–98

Firth CR, Stewart IS (2000) Postglacial tectonics of the Scottish glacio-isostatic uplift centre. Quatern Sci Rev 19(14–15):1469–1493

Foster C, Pennington CVL, Culshaw MG, Lawrie K (2012) The National Landslide Database of Great Britain: development, evolution and applications. Environ Earth Sci 66(3):941–953. https://doi.org/10.1007/s12665-011-1304-5

Frattini P, Crosta GB (2013) The role of material properties and landscape morphology on landslide size distributions. Earth Planet Sci Lett 361:310–319

Galli M, Ardizzone F, Cardinali M, Guzzetti F, Reichenbach P (2008) Comparing landslide inventory maps. Geomorphology 94(3–4):268–289

Gelman A, Hwang J, Vehtari A (2014) Understanding predictive information criteria for Bayesian models. Stat Comput 24(6):997–1016

Giles DP (2020) Chapter 1 introduction to geological hazards in the UK: their occurrence, monitoring and mitigation. Geol Soc London Eng Geol Spec Publ 29(1):1–41. https://doi.org/10.1144/EGSP29.1

Goetz JN, Brenning A, Petschko H, Leopold P (2015) Evaluating machine learning and statistical prediction techniques for landslide susceptibility modeling. Comput Geosci 81:1–11

Guttorp P, Gneiting T (2006) Studies in the history of probability and statistics XLIX on the Matérn correlation family. Biometrika 93(4):989–995

Guzzetti F, Carrara A, Cardinali M, Reichenbach P (1999) Landslide hazard evaluation: a review of current techniques and their application in a multi-scale study, Central Italy. Geomorphology 31(14):181–216

Guzzetti F, Galli M, Reichenbach P, Ardizzone F, Cardinali MJNH (2006) Landslide hazard assessment in the Collazzone area, Umbria, Central Italy. Nat Hazard 6(1):115–131

Guzzetti F, Mondini AC, Cardinali M, Fiorucci F, Santangelo M, Chang KT (2012) Landslide inventory maps: New tools for an old problem. Earth Sci Rev 112(1–2):42–66

Guzzetti F, Gariano SL, Peruccacci S, Brunetti MT, Marchesini I, Rossi M, Melillo M (2020) Geographical landslide early warning systems. Earth Sci Rev 200:102973

Heerdegen RG, Beran MA (1982) Quantifying source areas through land surface curvature. J Hydrol 57(3–4):359–373

Hill LJ, Sparks RSJ, Rougier JC (2013) Risk assessment and uncertainty in natural hazards. Risk and uncertainty assessment for natural hazards, edited by: Rougier, JC, Sparks, RS J., and Hill, LJ, pp.1–18. https://doi.org/10.1017/CBO9781139047562.002

Hosmer DW, Lemeshow S, Sturdivant RX (2000) Introduction to the logistic regression model. Appl Logist Regression 2:1–30

Hungr O, Leroueil S, Picarelli L (2014) The Varnes classification of landslide types, an update. Landslides 11:167–194

Illian JB, Hendrichsen DK (2010) Gibbs point process models with mixed effects. Environmetrics: Off J Int Environmetrics Soc 21(3–4):341–353

Illian J, Penttinen A, Stoyan H, Stoyan D (2008) Statistical analysis and modelling of spatial point patterns. John Wiley & Sons

Illian JB, Sørbye SH, Rue H (2012) A toolbox for fitting complex spatial point process models using Integrated Nested Laplace Approximation (INLA). Ann Appl Stat 6(4):1499–1530. https://doi.org/10.1214/11-AOAS530

Technologies I (2007) Dataset collection record: nextmap British digital terrain model dataset produced by intermap. Available at: http://catalogue.ceda.ac.uk/uuid/8f6e1598372c058f07b0aeac2442366d. Accessed 17 Sept 2024

Iverson RM (1997) The physics of debris flows. Rev Geophys 35(3):245–296

Korup O (2021) Bayesian geomorphology. Earth Surf Proc Land 46(1):151–172

Lari S, Frattini P, Crosta GB (2014) A probabilistic approach for landslide hazard analysis. Eng Geol 182:3–14

Lima P, Steger S, Glade T, Tilch N, Schwarz L, Kociu A (2017) Landslide susceptibility mapping at national scale: a first attempt for Austria. Advancing culture of living with landslides: volume 2 advances in landslide science. Springer International Publishing, Cham, pp 943–951

Lima P, Steger S, Glade T (2021) Counteracting flawed landslide data in statistically based landslide susceptibility modelling for very large areas: a national-scale assessment for Austria. Landslides 18(11):3531–3546

Lin Q, Lima P, Steger S, Glade T, Jiang T, Zhang J, Liu T, Wang Y (2021) National-scale datadriven rainfall induced landslide susceptibility mapping for China by accounting for incomplete landslide data. Geosci Front 12(6):101248

Lindgren F, Rue H, Lindström J (2011) An explicit link between Gaussian fields and Gaussian Markov random fields: the stochastic partial differential equation approach. Stat Methodol 73:423–498

Lindgren F, Rue H (2015) Bayesian spatial modelling with R-INLA. J Stat Softw 63(19):1–25. https://doi.org/10.18637/jss.v063.i19

Liu Z, Rue H (2022) Leave-group-out cross-validation for latent gaussian models. arXiv preprint arXiv:2210.04482. https://doi.org/10.48550/arXiv.2210.04482

Lombardo L, Cama M, Maerker M, Rotigliano E (2014) A test of transferability for landslides susceptibility models under extreme climatic events: application to the Messina 2009 disaster. Nat Hazards 74:1951–1989

Lombardo L, Opitz T, Huser R (2018) Point process-based modelling of multiple debris flow landslides using INLA: an application to the 2009 Messina disaster. Stoch Env Res Risk Assess 32:2179–2198

Lombardo L, Bakka H, Tanyas H, van Westen C, Mai PM, Huser R (2019) Geostatistical modelling to capture seismic-shaking patterns from earthquake-induced landslides. J Geophys Res Earth Surf 124(7):1958–1980

Lombardo L, Opitz T, Ardizzone F, Guzzetti F, Huser R (2020a) Space-time landslide predictive modelling. Earth-Sci Rev 209:103318

Lombardo L, Tanyas H, Nicu IC (2020b) Spatial modeling of multi-hazard threat to cultural heritage sites. Eng Geol 277:105776

Lombardo L, Tanyas H, Huser R, Guzzetti F, Castro-Camilo D (2021) Landslide size matters: A new data-driven, spatial prototype. Eng Geol 293:106288

Lv L, Chen T, Dou J, Plaza A (2022) A hybrid ensemble-based deep-learning framework for landslide susceptibility mapping. Int J Appl Earth Obs Geoinf 108:102713

Martha TR, van Westen CJ, Kerle N, Jetten V, Kumar KV (2013) Landslide hazard and risk assessment using semi-automatically created landslide inventories. Geomorphology 184:139–150

Martino S, Rue H (2009) Implementing approximate Bayesian inference using integrated nested Laplace approximation: a manual for the inla program. Department of Mathematical Sciences, NTNU, Norway

McKirdy A, Crofts R (1999) Scotland—the creation of its natural landscape. A Landscape Fashioned by Geology, Scottish Natural Heritage, Perth

Meyer R (2014) Deviance information criterion (DIC). Wiley StatsRef: Statistics Reference Online, pp.1-6. https://doi.org/10.1002/9781118445112.stat07878

Milne FD, Brown MJ, Davies MCR, Cameron G (2015) Some key topographic and material controls on debris flows in Scotland. Q J Eng GeolHydrogeol 48(3–4):212–223

Moreno M, Lombardo L, Crespi A, Zellner PJ, Mair V, Pittore M, van Westen C, Steger S (2024) Space-time data-driven modeling of precipitation-induced shallow landslides in South Tyrol, Italy. Sci Total Environ 912:169166

Moreno M, Steger S, Tanyas H, Lombardo L (2023) Modeling the area of co-seismic landslides via data-driven models: the Kaikōura example. Eng Geol 320:107121. https://doi.org/10.1016/j.enggeo.2023.107121

Nava L, Carraro E, Reyes-Carmona C, Puliero S, Bhuyan K, Rosi A, Monserrat O, Floris M, Meena SR, Galve JP, Catani F (2023) Landslide displacement forecasting using deep learning and monitoring data across selected sites. Landslides 20(10):2111–2129

Neteler M, Mitasova H (2013) Open source GIS: a GRASS GIS approach, vol 689. Springer Science & Business Media. https://doi.org/10.1007/978-0-387-68574-8

Novellino A, Cigna F, Brahmi M, Sowter A, Bateson L, Marsh S (2017) Assessing the feasibility of a national InSAR ground deformation map of Great Britain with Sentinel-1. Geosciences 7(2):19. https://doi.org/10.3390/geosciences7020019

Opitz T, Huser R, Bakka H, Rue H (2018) INLA goes extreme: Bayesian tail regression for the estimation of high spatio-temporal quantiles. Extremes 21(3):441–462

Ozturk U, Pittore M, Behling R, Roessner S, Andreani L, Korup O (2021) How robust are landslide susceptibility estimates? Landslides 18:681–695

Palamakumbura R, Finlayson A, Ciurean R, Nedumpallile-Vasu N, Freeborough K, Dashwood C (2021) Geological and geomorphological influences on a recent debris flow event in the Ice-scoured mountain quaternary domain, western Scotland. Proc

Geol' Assoc 132(4):456–468. https://doi.org/10.1016/j.pgeola.2021.05.002

Pennington C, Freeborough K, Dashwood C, Dijkstra T, Lawrie K (2015) The national landslide database of Great Britain: acquisition, communication and the role of social media. Geomorphology 249:44–51. https://doi.org/10.1016/j.geomorph.2015.03.013

Pudasaini SP, Krautblatter M (2022) The landslide velocity. Earth Surf Dyn 10(2):165–189

Rue H, Martino S, Chopin N (2009) Approximate Bayesian inference for latent Gaussian models by using integrated nested Laplace approximations. Stat Methodol 71:319–392

Rue H, Riebler A, Sørbye SH, Illian JB, Simpson DP, Lindgren FK (2017) Bayesian computing with INLA: a review. Annu Rev Stat Appl 4:395–421

Scheip C, Wegmann K (2022) Insights on the growth and mobility of debris flows from repeat high-resolution lidar. Landslides 19(6):1297–1319

Soeters R, Van Westen CJ (1996) Slope instability recognition, analysis and zonation. Transportation research board special report 247. National Research Council, National Academy Press, Washington, D. C., pp 129–177

Sosio R, Crosta GB, Frattini P (2007) Field observations, rheological testing and numerical modelling of a debris-flow event. Earth Surf Proc Land 32(2):290–306

Steger S, Brenning A, Bell R, Glade T (2016) The propagation of inventory-based positional errors into statistical landslide susceptibility models. Nat Hazard 16(12):2729–2745

Steger S, Mair V, Kofler C, Pittore M, Zebisch M, Schneiderbauer S (2021) Correlation does not imply geomorphic causation in data-driven landslide susceptibility modelling–Benefits of exploring landslide data collection effects. Sci Total Environ 776:145935

Stein ML (1999) Interpolation of spatial data: some theory for kriging. Springer Science & Business Media, New York

Steyerberg EW, Eijkemans MJ, Habbema JDF (1999) Stepwise selection in small data sets: a simulation study of bias in logistic regression analysis. J Clin Epidemiol 52(10):935942

Tang H, Hu X, Xu C, Li C, Yong R, Wang L (2014) A novel approach for determining landslide pushing force based on landslide-pile interactions. Eng Geol 182:15–24

Tanyas H, Kevin H, Luke M, Islam F, Luigi L (2022) Lessons learnt from the landslides triggered during and after the 2018 Mw 7.5 Papua New Guinea earthquake. In EGU general assembly conference abstracts (pp. EGU22–13472). https://doi.org/10.5194/egusphere-egu22-13472

Tanyas H, Lombardo L (2020) Completeness index for earthquake-induced landslide inventories. Eng Geol 264:105331

Taylor FE, Malamud BD, Witt A, Guzzetti F (2018) Landslide shape, ellipticity and length-towidth ratios. Earth Surf Proc Land 43(15):3164–3189

Turel M, Frost JD (2011) Delineation of slope profiles from digital elevation models for landslide hazard analysis. In Geo-risk 2011: Risk assessment and management (pp. 829–836). https://doi.org/10.1061/41183(418)87

Van den Bout B, Lombardo L, Chiyang M, van Westen C, Jetten V (2021) Physically-based catchment-scale prediction of slope failure volume and geometry. Eng Geol 284:105942

Van Niekerk J, Krainski E, Rustand D, Rue H (2023) A new avenue for Bayesian inference with INLA. Comput Stat Data Anal 181:107692

Van Westen CJ, Castellanos E, Kuriakose SL (2008) Spatial data for landslide susceptibility, hazard, and vulnerability assessment: an overview. Eng Geol 102(3–4):112–131

Winter MG, Dent J, Macgregor F, Dempsey P, Motion A Shackman L (2010) Debris flow, rainfall and climate change in Scotland. Geological Society of London. https://doi.org/10.1144/1470-9236/08-108

Erin Bryce (✉) · **Daniela Castro-Camilo**
Department of Mathematics and Statistics, University of Glasgow, Glasgow, UK

Erin Bryce
Email: 2313549b@student.gla.ac.uk

Claire Dashwood · Roxana Ciurean · Alessandro Novellino
British Geological Survey, Nicker Hill, Keyworth NG12 5GG, UK

Hakan Tanyas · Luigi Lombardo
AES Department, ITC, Faculty of Geo-Information Science and Earth Observation, University of Twente, Enschede, The Netherlands